TMEM55B controls lipolysis via lysosomal pH and ER–lysosome calcium signaling

Nagi Mukae[1], Honoka Maki[1] & Michiko Shirane[1]*

[1]Department of Molecular Biology, Graduate School of Pharmaceutical Sciences, Nagoya City University, Nagoya, Aichi, Japan.

*Corresponding: M.S. (shiram@phar.nagoya-cu.ac.jp)

Keywords:
TMEM55B, PDZD8, Lysosomes, Endoplasmic reticulum, Calcium, Membrane contact sites

ABSTRACT

Endolysosomal maturation is accompanied by luminal acidification and increased Ca^{2+} concentration. Mature lysosomes function as major intracellular Ca^{2+} storage organelles, alongside the endoplasmic reticulum (ER) and mitochondria. Recent studies have highlighted a role for lysosomal Ca^{2+} in calcium-induced calcium release (CICR), where local lysosomal Ca^{2+} efflux triggers subsequent ER Ca^{2+} release at ER–lysosome membrane contact sites (MCSs). However, the molecular mechanisms underlying this process remain incompletely understood. In this study, we identified the lysosome-localized protein TMEM55B in a PDZD8-associated protein complex, a factor previously implicated in lipid transfer and membrane tethering at ER–late endosome/lysosome (LE/Ly) contacts. Loss of TMEM55B disrupted lysosomal acidification and impaired lipid droplet degradation. TMEM55B knockdown also reduced lysosomal Ca^{2+} release and uptake, accompanied by attenuated CICR at ER–LE/Ly MCSs. Together, these findings suggest that TMEM55B contributes to the regulation of lysosomal pH and Ca^{2+} dynamics and may influence Ca^{2+} signaling between lysosomes and the ER.

Introduction

ER- LE/Ly MCSs are not formed by random contacts between the ER and endosomes but are mediated by specific membrane tethering complexes. ORP1L and VAP were first identified as tethering factors of ER–LE/Ly MCSs, and subsequent studies revealed that many sterol transfer proteins—including ORP, STARD, and Lam families, as well as NPC1, Protrudin, and PDZD8—also function at these sites[1-3]. The tethering of ER–LE/Ly MCSs is strengthened during endosomal maturation, a process involving both endosomal acidification and Ca^{2+} dynamics. Cholesterol and Ca^{2+} therefore serve as key messengers mediating cross-talk between these two organelles at ER–LE/Ly MCSs[4].

Cells acquire cholesterol through two main pathways: de novo synthesis and endocytosis of lipoproteins (LPs)[5-7]. In the brain, however, neurons lack the ability to synthesize cholesterol and instead rely on supply from glial cells. Cholesterol produced in glia is esterified to cholesteryl esters (CEs), packed into HDL-like lipoproteins, transported to neurons, internalized via LDLR-mediated endocytosis, and hydrolyzed to free cholesterol by lysosomal acidic lipases[7,8]. This cholesterol is then trafficked to the ER and redistributed to other organelles for cellular functions[4,9].

CEs stored in lipid droplets (LDs) are degraded through lipophagy, a form of microautophagy in which LDs fuse with lysosomes, enabling lipids to be hydrolyzed by

53 lysosomal acidic lipases[10-13]. Endocytosed LP particles are degraded in a similar manner.
54 Thus, endosomal maturation, which depends on lysosomal acidification, is essential for
55 metabolizing CEs from both LDs and LPs into cholesterol.
56 PDZD8 is an ER membrane protein originally identified as a Protrudin-binding partner,
57 with both proteins acting as tethers at ER–LE/Ly MCSs[14-21]. PDZD8 belongs to the
58 TULIP super family and mediates cholesterol transport through its SMP domain[16,22,23].
59 Because Protrudin interacts with VAP via its FFAT motif, the PDZD8–Protrudin–VAP
60 complex is thought to function in lipid transport[3]. PDZD8 thereby contributes to
61 cholesterol metabolism by promoting lipolysis through endosomal maturation in
62 neurons[24]. Consistently, PDZD8-deficient mice exhibit CE accumulation in the brain due
63 to impaired lipolysis, along with memory and emotional dysfunction[25,26]. CE
64 accumulation is also observed in the brains of Alzheimer's disease (AD) patients and AD
65 model mice[27-29]. In particular, neurons carrying the APOE4 allele—the strongest genetic
66 risk factor for AD—show CE accumulation with lipofuscin formation due to impaired
67 lysosomal function[30,31].
68 Compared with cholesterol metabolism, research on lysosomal calcium dynamics is
69 relatively recent, and many questions remain unresolved. As endosomes undergo luminal
70 acidification, their Ca^{2+} concentration increases, and lysosomes eventually become a
71 major intracellular Ca^{2+} store alongside the ER and mitochondria. Ca^{2+} uptake into the
72 endosomal lumen promotes intraluminal vesicle fusion, thereby facilitating endosomal
73 maturation[32-35]. Conversely, calcium-induced calcium release (CICR)—in which a small
74 amount of Ca^{2+} efflux from lysosomes trigger large scale release from the ER IP_3
75 receptors and ryanodine receptors—has emerged as an important mechanism of transient
76 Ca^{2+} signaling[36-40]. Endosomal acidification activates lysosomal Ca^{2+} channels, such as
77 two-pore channel-2 (TPC2) and TRPML1, which promote Ca^{2+} release from lysosomes.
78 Although Ca^{2+} dynamics at ER–LE/Ly MCSs have been implicated in diverse cellular
79 processes[35,41], their detailed mechanisms remain poorly understood.
80 TMEM55B has been reported to perform multiple functions. It was first identified as a
81 phosphatase that hydrolyzes the 4-position phosphate of PtdIns(4,5)P_2 to generate
82 PtdIns(5)P[42,43]. TMEM55B is a lysosomal membrane protein that interacts with the v-
83 ATPase and Ragulator complexes, thereby contributing to v-ATPase activation and
84 subsequent mTORC1 signaling at the lysosomal membrane[44]. Consistent with its
85 importance, TMEM55B knockout mice are embryonic lethal[44]. Because v-ATPase is a
86 proton pump essential for endolysosomal acidification, its dysfunction leads to various
87 lysosomal storage diseases[45-47]. TMEM55B also cooperates with TFEB and JIP4 to
88 promote dynein-dependent retrograde lysosomal transport[48] and participate in lysosomal

89 oxidative stress responses[49]. In addition, TMEM55B regulates the expression and activity
90 of LDLR thereby modulating lipoprotein uptake and cholesterol metabolism[50,51].
91 In this study, we identified lysosomal protein TMEM55B in a PDZD8 complex that may
92 regulate cholesterol metabolism via lysosomal acidification and Ca^{2+} dynamics at ER–
93 LE/Ly MCSs.
94
95 **Results**
96 **Identification of lysosomal protein TMEM55B in the PDZD8 complex.**
97 In neuronal cells, the lipid transfer protein PDZD8 promotes cholesterol metabolism via
98 endosomal maturation; however, the mechanism by which this ER protein regulates
99 lysosomal activity remains unclear. To identify lysosomal proteins interacting with
100 PDZD8, we established a Neuro2A cell line stably expressing 3×FLAG-tagged PDZD8.
101 The PDZD8 complex was isolated by anti-FLAG immunoprecipitation, separated by
102 SDS-PAGE, digested with trypsin, and analyzed by LC-MS/MS. In parallel, the same
103 analysis was performed using cells transfected with empty vector to exclude nonspecific
104 binding. Proteins reproducibly detected across three independent experiments were
105 extracted, and semiquantitative analysis based on identification frequency (IF)[52]
106 identified 196 proteins with IF > 0.01. Among those, 13 endosome-localized proteins
107 were selected using GO Term and UniProt subcellular localization annotations (Fig. 1A).
108 This group included the lysosomal protein TMEM55B and its binding partners, v-ATPase
109 subunit Atp6v0d1 and Lamtor1 (Fig. 1A)[44]. Notably, Lamtor1 and TMEM55B are
110 lysosome-localized proteins associated with cholesterol metabolism, suggesting a
111 potential role in lipolysis-mediated cholesterol processing. Since TMEM55B regulates
112 the v-ATPase complex, we focused on TMEM55B as a possible upstream regulator of
113 PDZD8-mediated lysosomal function.
114
115 **TMEM55B is not essential for ER–LE/Ly tethering.**
116 Because PDZD8 functions as a tether at ER–LE/Ly MCSs, we examined whether its
117 binding partner TMEM55B also contributes to this process. TMEM55B expression was
118 suppressed in HeLa cells using siRNA (siTMEM55B), resulting in a marked reduction of
119 both RNA and protein levels compared with control cells (siControl) (Fig. 1B, C). To
120 assess ER–LE/Ly contacts, we employed a split-GFP system in which GFP fluorescence
121 is reconstituted only when ER and lysosomal membranes are closely apposed[16,53]. Cells
122 were co-transfected with ERj1-GFP(1–10) (ER-localized fragment) and LAMP1-
123 GFP(11) (lysosomal fragment), together with mCherry to normalize expression levels.
124 The GFP/mCherry fluorescence ratio per cell, reflecting ER–LE/Ly MCS formation, was

125 quantified (Fig. 1D). No significant difference in GFP/mCherry ratio was observed
126 between siTMEM55B and siControl cells (Fig. 1E). Compared with prior reports,
127 including our own showing reduced ER–LE/Ly tethering upon Protrudin or PDZD8
128 knockdown, TMEM55B knockdown caused only a minor effect, suggesting it is unlikely
129 a major contributor to tethering of ER–LE/Ly MCSs.
130

131 **TMEM55B regulates lysosomal acidification and activity.**

132 TMEM55B interacts with the v-ATPase complex and has been implicated in its regulation.
133 We therefore hypothesized that TMEM55B contributes to lysosomal acidification and
134 activity via v-ATPase. To test this, HeLa cells transfected with siControl or siTMEM55B
135 were stained with LysoTracker (Fig. 2A) or LysoSensor (Fig. 2C), both of which increase
136 in fluorescence intensity as lysosomal pH decreases. In both assays, siTMEM55B cells
137 showed significantly reduced fluorescence compared with controls, indicating impaired
138 lysosomal acidification (Fig. 2B, D). To assess the functional consequences in neurons,
139 we suppressed TMEM55B expression in PC12 cells (Fig. 2E) and evaluated lipolysis
140 using EGFP-PLIN2 as a lipid droplet (LD) marker and LysoTracker Red as a lysosomal
141 marker (Fig. 2F). TMEM55B knockdown cells exhibited enlarged LDs (Fig. 2G) with
142 increased LD fluorescence intensity per cell (Fig. 2H), as well as reduced LysoTracker
143 fluorescence (Fig. 2I), consistent with defective lysosomal acidification and impaired
144 lipolysis. Furthermore, LD–lysosome fusion events were significantly decreased in
145 siTMEM55B cells compared with controls (Fig. 2J). Together, these results demonstrate
146 that TMEM55B may promote lysosomal acidification and activity, thereby facilitating
147 LD degradation and lipolysis. However, since the signals from the Lysotracker and
148 Lysosensor alone cannot reliably quantify lysosomal pH, a colorimetric probe that
149 directly measures lysosomal pH would be useful.
150

151 **TMEM55B promotes Ca^{2+} release from the ER.**

152 Intracellular Ca^{2+} elevation promotes lysosome fusion with other organelles[45], suggesting
153 that lipolysis mediated by the PDZD8–TMEM55B complex could involve Ca^{2+} signaling
154 at ER–LE/Ly MCSs. Since the ER is the major intracellular Ca^{2+} store, we investigated
155 whether TMEM55B regulates Ca^{2+} release or uptake from the ER. HeLa cells were
156 transfected with the ER-targeted Ca^{2+} indicator G-CEPIA1er[54], which binds ER luminal
157 Ca^{2+} and emits GFP fluorescence, and colocalization with the ER marker KDEL was
158 confirmed by confocal microscopy (Fig. 3A, B). To assess ER Ca^{2+} dynamics, siControl
159 or siTMEM55B cells were stimulated with ATP to induce transient ER Ca^{2+} release,
160 followed by Ca^{2+} reuptake to the ER. In siTMEM55B cells, ATP-induced Ca^{2+} release as

161 well as reuptake were markedly reduced compared with controls (Fig. 3C, D).
162 Quantitative analysis revealed that siTMEM55B cells exhibited significantly decreased
163 rates of ER Ca^{2+} release (Fig. 3E), slower subsequent Ca^{2+} reuptake (Fig. 3F), and delayed
164 time to peak Ca^{2+} release (Fig. 3G). These findings indicate that TMEM55B may
165 facilitates ATP-stimulated transient Ca^{2+} release from the ER.
166

167 **TMEM55B promotes Ca^{2+} release from lysosomes.**

168 We next investigated whether TMEM55B regulates Ca^{2+} release from lysosomes and how
169 this affects ER Ca^{2+} dynamics. Lysosomal Ca^{2+} release and uptake were monitored using
170 Ly-GG, which binds cytosolic Ca^{2+} at the lysosomal membrane and emits GFP
171 fluorescence[55] (Fig. 4A). Co-expression of Ly-GG with the lysosomal marker LAMP1
172 confirmed colocalization (Fig. 4B). ATP stimulation of siControl HeLa cells induced
173 transient Ca^{2+} release from lysosomes. In siTMEM55B cells, the magnitude (Fig. 4C) and
174 rate (Fig. 4D) of lysosomal Ca^{2+} release were significantly reduced compared to controls.
175 The subsequent Ca^{2+} reuptake rate was also decreased (Fig. 4E), indicating impaired
176 lysosomal Ca^{2+} dynamics. As a control, we examined mitochondrial Ca^{2+} using
177 CEPIA3mt[54], which binds mitochondrial matrix Ca^{2+}, together with the mitochondrial
178 marker Su9-RFP[56] (Fig. 4F), confirmed colocalization (Fig. 4G). ATP stimulation
179 induced transient mitochondrial Ca^{2+} increases as well as decrease, which were not
180 significantly different between siControl and siTMEM55B cells (Fig. 4H–J). These
181 results indicate that TMEM55B may specifically regulates lysosomal Ca^{2+} dynamics
182 without affecting mitochondrial Ca^{2+}.
183

184 **Discussion**

185 Lysosomes serve as central hubs for cellular metabolism, coordinating degradation,
186 nutrient recycling, and signaling. Proper lysosomal acidification and calcium homeostasis
187 are essential for lipid metabolism and neuronal function, and their dysregulation has been
188 increasingly linked to neurodegenerative diseases. Despite this, the molecular
189 mechanisms connecting lysosomal function to lipid regulation remain incompletely
190 understood.
191 In this study, we identify TMEM55B as a key lysosomal regulator that interacts with the
192 ER protein PDZD8 to control lysosomal acidification and calcium dynamics. Through
193 these functions, TMEM55B in PDZD8 complex may contribute to endosomal maturation
194 and lipid droplet degradation, revealing a novel mechanism linking lysosomal activity to
195 lipid metabolism. These findings provide new insights into cellular lipid homeostasis and

196 suggest potential targets for disorders associated with lysosomal dysfunction and
197 cholesterol metabolism.
198 However, immunoprecipitation-immunoblotting analysis of endogenous proteins
199 yielded signals below the detection threshold, and that of overexpressed exogenous
200 proteins resulted in non-specific interactions, preventing us from demonstrating direct
201 binding between TMEM55B and PDZD8. Therefore, while both proteins reside within
202 the same complex, the interaction may be indirect rather than direct, and TMEM55B-
203 dependent regulation of lysosomal acidification and calcium dynamics may occur
204 independently of PDZD8.
205 Because Ly-GG can detect Ca^{2+} originating from the ER in proximity to lysosomes,
206 reduced ER-derived local Ca^{2+} release may also contribute to the decreased Ly-GG signal
207 following TMEM55B knockdown.
208 The lipid transfer protein PDZD8 mediates tethering of ER–LE/Ly membrane contact
209 sites (MCSs) and facilitates cholesterol metabolism through lipolysis via endosomal
210 maturation. However, the mechanism by which PDZD8 promotes endosome maturation
211 has remained unclear. Through complex analysis in neuronal cells, we identified Lamtor1
212 and TMEM55B as lysosome-localized, cholesterol-associated proteins among LE/Ly
213 candidates. Given that TMEM55B regulates the v-ATPase complex, we focused on its
214 intracellular functions.
215 We found that TMEM55B contributes to lysosomal acidification and activation. Loss of
216 TMEM55B impaired lysosomal Ca^{2+} release and uptake, as well as ATP-stimulated Ca^{2+}
217 release from the ER, while mitochondrial Ca^{2+} dynamics remained unaffected. In our
218 system, lysosomal Ca^{2+} release peaked within 180 s after ATP stimulation (Fig. 4C),
219 whereas ER Ca^{2+} release peaked later (Fig. 3C), consistent with calcium-induced calcium
220 release (CICR) from the ER triggered by lysosomal Ca^{2+} release. These results indicate
221 that TMEM55B promotes endosomal maturation via lysosomal acidification and
222 activation, and facilitates CICR at ER–LE/Ly MCSs, thereby supporting lipolysis (Fig.
223 5).
224 The PDZD8–TMEM55B complex thus plays a central role in ER–LE/Ly MCS functions,
225 including endosomal maturation, Ca^{2+} dynamics, and cholesterol metabolism.
226 Nevertheless, the effects of TMEM55B deficiency on lysosomal fusion and lipid droplet
227 degradation were partial, failing to recapitulate the strong phenotype observed with
228 PDZD8 deficiency. This suggests that additional, as-yet-unidentified mechanisms
229 contribute to PDZD8-mediated lipolysis.
230 In summary, TMEM55B enhances lysosomal acidification via v-ATPase regulation,
231 thereby increasing lysosomal enzyme activity and promoting lipolysis. Lysosomal

232 acidification also activates Ca^{2+} channels, facilitating CICR at ER–LE/Ly MCSs and
233 supporting cholesterol metabolism through lysosomal fusion. Direct evidence linking
234 TMEM55B-mediated CICR to enhanced lipolysis, however, remains lacking, and further
235 studies are needed to clarify this mechanism.
236
237 **Limitation of this study**
238 We were unable to demonstrate direct binding between endogenous or exogenous PDZD8
239 and TMEM55B proteins. Attempts to express TMEM55B at endogenous levels for rescue
240 experiments were also unsuccessful. Additionally, assessing V-ATPase assembly
241 following TMEM55B knockdown proved technically difficult and was beyond the scope
242 of this work. Although TMEM55B deficiency caused partial defects in lysosomal fusion
243 and lipid droplet degradation, the phenotype was less pronounced than that observed with
244 PDZD8 loss. These findings imply that additional, unidentified mechanisms may
245 contribute to PDZD8-dependent lipolysis, which remain unresolved in this study.
246
247 **Methods**
248 **Plasmids**
249 EGFP and mCherry vectors were from Clontech (Mountain View, CA, US). Human
250 cDNAs encoding PLIN2 (GenBank accession number NM_007408.4), LAMP1
251 (GenBank accession number BC025335), and KDEL with the signal sequence of
252 calreticulin (GenBank accession number NM_004343) were amplified from HeLa cells
253 by the polymerase chain reaction (PCR) with PrimeSTAR HS DNA polymerase (Takara,
254 Shiga, Japan). pCMV-G-CEPIA1er (Addgene plasmid #58215) and pCMV-CEPIA3mt
255 (Addgene plasmid #58219) were obtained from Addgene (Watertown, MA, US). Ly-GG
256 was kindly provided by Dr. CW Taylor (University of Cambridge, UK). Vectors for split-
257 GFP analysis, ERj1–GFP(1–10) and LAMP1–GFP(11), were kindly provided by Dr.
258 Tamura (Yamagata University, Japan). The pSu9 cDNA was kindly provided by Dr.
259 Mihara (Kyushu University, Japan). The mRFP cDNA was kindly provided by Dr. R.Y.
260 Tsien (University of California, San Diego, US).
261
262 **Antibodies**
263 Antibodies to TMEM55B were from Proteintech (Rosemont, IL, USA); antibodies to
264 HSP90 were from BD Biosciences (Franklin Lakes, NJ, USA).
265
266 **Cell culture, transfection, and retrovirus infection**

267 HeLa cells (CCL-2, purchased from ATCC, US) were cultured under a humidified
268 atmosphere of 5% CO_2 at 37°C in Dulbecco's modified Eagle's medium (Invitrogen Life
269 Technologies) supplemented with 10% fetal bovine serum (Invitrogen Life Technologies).
270 The culture medium for Plat-E cells was also supplemented with blasticidin (10 μg/ml).
271 Cells were transfected with the use of XtremeGene9 reagents (Roche Diagnostics,
272 Mannheim, Germany) according to the manufacturer's protocol. For retroviral infection,
273 Plat-E cells were transiently transfected with pMX-puro–based vectors and then cultured
274 for 48 h. The retroviruses in the resulting culture supernatants were used to infect
275 Neuro2A cells, and the cells were then subjected to selection with puromycin (1 μg/ml).
276

277 **Identification and categorization of PDZD8-associated proteins**

278 Neuro2a cells infected with a retrovirus encoding FLAG–tagged mouse PDZD8 or with
279 the corresponding empty virus were solubilized in a lysis buffer (40 mM HEPES-NaOH
280 [pH 7.5], 150 mM NaCl, 10% glycerol, 0.5% Triton X-100, 1 mM Na_3VO_4, 25 mM NaF,
281 aprotinin [10 μg/ml], leupeptin [10 μg/ml], 1 mM phenylmethylsulfonyl fluoride) to
282 prepare whole-cell extracts. Lysates were cleared by centrifugation at 20,400 × g for 15
283 min at 4 °C. The clarified supernatants were subjected to affinity purification with anti-
284 FLAG (M2)–agarose affinity gel (Sigma-Aldrich), and then proteins eluted with FLAG
285 peptide (Sigma-Aldrich) was separated by SDS-PAGE and stained with silver. The
286 stained gels were sliced into pieces, and the abundant proteins therein were subjected to
287 in-gel digestion with trypsin. The resulting peptides were dried, dissolved in a mixture of
288 0.1% trifluoroacetic acid and 2% acetonitrile, and then applied to a nanoflow LC system
289 (Advanced UHPLC; Michrom BioResources, Auburn, CA, USA) equipped with an L-
290 column (C18, 0.15 by 50 mm, particle size of 3 μm; CERI, Tokyo, Japan). LC–MS/MS
291 analysis was performed with an Orbitrap Velos Pro instrument (Thermo Fisher Scientific).
292 All MS/MS spectra were compared with protein sequences in the International Protein
293 Index (IPI, European Bioinformatics Institute) mouse version 3.44 with the use of the
294 MASCOT algorithm. Assigned high-scoring peptide sequences were considered for
295 correct identification. Identified peptides from 3 independent experiments were integrated
296 and regrouped by IPI accession number. Proteins detected in ≥2 of 3 independent
297 experiments from FLAG-PDZD8–expressing cells, but absent from control cells, were
298 considered PDZD8-associated. Semi-quantitative abundance was estimated from
299 identification frequency (IF; number of identified peptides per protein normalized to the
300 number of theoretically detectable tryptic peptides). Functional categorization of
301 PDZD8-associated proteins was categorized with use of the UniProtKB database
302 (https://www.uniprot.org) based on Gene Ontology (GO) annotations. The proteins listed

303 in figure 1a shows endosome-related (GO:0005768), as well as columns for lysosome
304 (GO:0005764) or cholesterol-related as well.
305
306 **RNA interference, reverse transcription, and real-time PCR analysis**
307 Stealth siRNAs targeted to human TMEM55B (siTMEM55B#1, 5'-
308 ACGUGGAAGGCAAGAUGCAUCAGCA-3'; siTMEM55B#2, 5'-
309 CAAGAUGCAUCAGCAUGUAGUCAAA-3'), rat TMEM55B (siTMEM55B#1, 5'-
310 UGCUGAUGCAUCUUGCCUUCCACGU-3'; siTMEM55B#2, 5'-
311 CAAGAUGCAUCAGCAUGUAGUCAAA-3'), and non-targeting control were obtained
312 from Invitrogen Life Technologies. (Invitrogen Life Technologies, Carlsbad, CA, USA).
313 Human siRNAs were introduced into HeLa cells with the use of Lipofectamine
314 RNAiMAX (Invitrogen Life Technologies), and rat siRNAs were introduced into PC12
315 cells with the use of a Cell Line Nucleofector Kit V (VCA-1003) and Nucleofector
316 instrument (Lonza, Basel, Switzerland) according to the manufacturer's protocol. The
317 cells were then cultured for 48 h (for HeLa) or 72 h (for PC12). Total RNA was isolated
318 from cells with the use of an RNeasy Mini Kit (Qiagen, Hilden, Germany) according to
319 the manufacturer's protocol and was subjected to reverse transcription (RT) with the use
320 of a QuantiTect Rev Transcription Kit (Qiagen). The resulting cDNA was subjected to
321 real-time PCR analysis with Power SYBR Green PCR Master Mix in an ABI-Prism 7000
322 sequence detection system (Applied Biosystems, Foster City, CA). The amounts of each
323 target mRNA were calculated and normalized by that of GAPDH mRNA. Primers for
324 PCR (forward and reverse, respectively) were as follows: 5'-
325 GTCAGTGGTGGACCTGACCTG-3' and 5'-AAAGTGGTCGTTGAGGGCAAT-3' for
326 human GAPDH; 5'-CGAGTCTGCCAATCTCTCATC-3' and 5'-
327 AGTGCGGTCTGTGAACTCTGT-3' for human TMEM55B; 5'-
328 AAGGCTGAGAATGGGAAGCTG-3' and 5'-GGAGATGATGACCCTTTTGGC-3' for
329 rat GAPDH; 5'-CTAGCCCGGATAGTGGGAGTG-3' and 5'-
330 TTCCTGGAGGTGCATTCTTGA-3' for rat TMEM55B.
331
332 **Fluorescence imaging of live cells**
333 LysoTracker Red DND-99 (0.2 μM) or LysoSensor Green DND-189 (0.2 μM) (Thermo
334 Fisher Scientific, Rockford, IL, USA) were added to cells for 1 h at 37 °C according to
335 the manufacturer's protocol. HeLa and PC12 cells expressing plasmid-encoded
336 fluorescent proteins for 24 h and 96 h respectively, or metabolically labeled with
337 fluorescent probes were observed with an LSM800 confocal microscope (Zeiss,

338 Oberkochen, Germany), and the images were processed for calculation of fluorescence
339 intensity with ZEN imaging software (Zeiss) as well as Fiji (ImageJ, https://fiji.sc).
340

341 **Ca^{2+} imaging**

342 Cell media of HeLa cells expressing organelle-targeted Ca^{2+} indicators were pre-
343 incubated with HEPES-buffered saline (HBS; 137 mM NaCl, 5.9 mM KCl, 2.2 mM $CaCl_2$,
344 1.2 mM $MgCl_2$, 10 mM HEPES, 14 mM glucose, pH 7.4) for 1 h at 37 °C and then
345 stimulated with ATP (200 μM) (Wako, Japan). The images were captured by Operetta
346 high-content screening system (PerkinElmer, Waltham, MA, USA) using a ×20 objective
347 (λ_ex 460–490 nm; λ_em 500–550 nm) at the time point of ATP addition (t = 0 s) and
348 continued time points (t = X s) at a rate of one frame per 20 sec for total 1240 sec (G-
349 CEPIA) or 180 sec (Ly-GG and CEPIA3mt). The concentration of Ca^{2+} for each time
350 points was calculated by $\Delta F/F_0 = (F_x - F_0)/F_0$. Images were analyzed by Harmony
351 software (PerkinElmer).
352

353 **Immunoblot analysis**

354 HeLa cells were lysed in Triton lysis buffer containing 40 mM HEPES-NaOH (pH 7.6),
355 150 mM NaCl, 0.5% Triton X-100, 10 mM $MgCl_2$, 1 mM Na_3VO_4, 25 mM NaF, 1 mM
356 EDTA, 1 mM PMSF, leupeptin (10 μg/mL), and 10% glycerol. After 10 min on ice,
357 lysates were centrifuged at 15,000 × g for 10 min at 4 °C, and protein concentrations were
358 determined with the Pierce BCA Protein Assay (Thermo Fisher Scientific). Extracts were
359 resolved by SDS–PAGE, transferred to Immobilon-P membranes (Merck Millipore,
360 Darmstadt, Germany), and probed with primary antibodies. Signals were developed with
361 SuperSignal reagents (Thermo Fisher Scientific) and imaged on an LAS-4000 (GE
362 Healthcare, Waukesha, WI, USA).
363

364 **Statistical analysis**

365 Statistical analyses were performed with BellCurve for Excel software (Social Survey
366 Research Information, Tokyo, Japan). Normality of data was assessed with the Shapiro–
367 Wilk test. If the normality assumption was not met, the Kruskal–Wallis test with the
368 Steel's multiple comparisons test were applied. If data were normally distributed, One-
369 way repeated-measures analysis of variance (ANOVA) with the Dunnett's multiple
370 comparisons test were performed. Quantitative data are presented as mean ± SE.
371 Statistical significance of a *P* value is indicated as $0.01 \leq p < 0.05$ (*); $0.001 \leq p < 0.01$
372 (**); $p < 0.001$ (***); $p \geq 0.05$ (n.s.). Sample size (*n*) are in the figure legends.
373

374 **References**

375 1 Luo, J., Jiang, L. Y., Yang, H. & Song, B. L. Intracellular Cholesterol Transport
376 by Sterol Transfer Proteins at Membrane Contact Sites. *Trends Biochem Sci* **44**,
377 273-292, doi:10.1016/j.tibs.2018.10.001 (2019).
378 2 Wong, L. H., Gatta, A. T. & Levine, T. P. Lipid transfer proteins: the lipid
379 commute via shuttles, bridges and tubes. *Nat Rev Mol Cell Biol* **20**, 85-101,
380 doi:10.1038/s41580-018-0071-5 (2019).
381 3 Shirane, M. Lipid Transfer-Dependent Endosome Maturation Mediated by
382 Protrudin and PDZD8 in Neurons. *Front Cell Dev Biol* **8**, 615600,
383 doi:10.3389/fcell.2020.615600 (2020).
384 4 van der Kant, R. & Neefjes, J. Small regulators, major consequences - Ca(2)(+)
385 and cholesterol at the endosome-ER interface. *J Cell Sci* **127**, 929-938,
386 doi:10.1242/jcs.137539 (2014).
387 5 Ikonen, E. Cellular cholesterol trafficking and compartmentalization. *Nat Rev*
388 *Mol Cell Biol* **9**, 125-138, doi:10.1038/nrm2336 (2008).
389 6 Goldstein, J. L. & Brown, M. S. A century of cholesterol and coronaries: from
390 plaques to genes to statins. *Cell* **161**, 161-172, doi:10.1016/j.cell.2015.01.036
391 (2015).
392 7 Luo, J., Yang, H. & Song, B. L. Mechanisms and regulation of cholesterol
393 homeostasis. *Nat Rev Mol Cell Biol* **21**, 225-245, doi:10.1038/s41580-019-0190-
394 7 (2020).
395 8 Mehta, N. *et al.* The evolving role of cholesteryl ester transfer protein inhibition
396 beyond cardiovascular disease. *Pharmacol Res* **197**, 106972,
397 doi:10.1016/j.phrs.2023.106972 (2023).
398 9 Martin, M. G., Pfrieger, F. & Dotti, C. G. Cholesterol in brain disease:
399 sometimes determinant and frequently implicated. *EMBO Rep* **15**, 1036-1052,
400 doi:10.15252/embr.201439225 (2014).
401 10 Zechner, R., Madeo, F. & Kratky, D. Cytosolic lipolysis and lipophagy: two
402 sides of the same coin. *Nat Rev Mol Cell Biol* **18**, 671-684,
403 doi:10.1038/nrm.2017.76 (2017).
404 11 Schuck, S. Microautophagy - distinct molecular mechanisms handle cargoes of
405 many sizes. *J Cell Sci* **133**, doi:10.1242/jcs.246322 (2020).
406 12 Haidar, M., Loix, M., Bogie, J. F. J. & Hendriks, J. J. A. Lipophagy: a new
407 player in CNS disorders. *Trends Endocrinol Metab* **32**, 941-951,
408 doi:10.1016/j.tem.2021.08.010 (2021).

13 Lan, Z. Q., Ge, Z. Y., Lv, S. K., Zhao, B. & Li, C. X. The regulatory role of lipophagy in central nervous system diseases. *Cell Death Discov* **9**, 229, doi:10.1038/s41420-023-01504-z (2023).

14 Shirane, M. & Nakayama, K. I. Protrudin induces neurite formation by directional membrane trafficking. *Science* **314**, 818-821, doi:10.1126/science.1134027 (2006).

15 Guillen-Samander, A., Bian, X. & De Camilli, P. PDZD8 mediates a Rab7-dependent interaction of the ER with late endosomes and lysosomes. *Proc Natl Acad Sci U S A* **116**, 22619-22623, doi:10.1073/pnas.1913509116 (2019).

16 Shirane, M. *et al.* Protrudin and PDZD8 contribute to neuronal integrity by promoting lipid extraction required for endosome maturation. *Nat Commun* **11**, 4576, doi:10.1038/s41467-020-18413-9 (2020).

17 Elbaz-Alon, Y. *et al.* PDZD8 interacts with Protrudin and Rab7 at ER-late endosome membrane contact sites associated with mitochondria. *Nat Commun* **11**, 3645, doi:10.1038/s41467-020-17451-7 (2020).

18 Khan, H., Chen, L., Tan, L. & Im, Y. J. Structural basis of human PDZD8-Rab7 interaction for the ER-late endosome tethering. *Sci Rep* **11**, 18859, doi:10.1038/s41598-021-98419-5 (2021).

19 Gao, Y., Xiong, J., Chu, Q. Z. & Ji, W. K. PDZD8-mediated lipid transfer at contacts between the ER and late endosomes/lysosomes is required for neurite outgrowth. *J Cell Sci* **135**, doi:10.1242/jcs.255026 (2022).

20 Thakur, R. S. & O'Connor-Giles, K. M. PDZD8 promotes autophagy at ER-lysosome membrane contact sites to regulate activity-dependent synaptic growth. *Cell Rep* **44**, 115483, doi:10.1016/j.celrep.2025.115483 (2025).

21 Yang, H. *et al.* LYVAC/PDZD8 is a lysosomal vacuolator. *Science* **389**, eadz0972, doi:10.1126/science.adz0972 (2025).

22 Alva, V. & Lupas, A. N. The TULIP superfamily of eukaryotic lipid-binding proteins as a mediator of lipid sensing and transport. *Biochim Biophys Acta* **1861**, 913-923, doi:10.1016/j.bbalip.2016.01.016 (2016).

23 Wong, L. H. & Levine, T. P. Tubular lipid binding proteins (TULIPs) growing everywhere. *Biochim Biophys Acta Mol Cell Res* **1864**, 1439-1449, doi:10.1016/j.bbamcr.2017.05.019 (2017).

24 Morita, K. *et al.* PDZD8-deficient mice accumulate cholesteryl esters in the brain as a result of impaired lipophagy. *iScience* **25**, 105612, doi:10.1016/j.isci.2022.105612 (2022).

25 Al-Amri, A. H. *et al.* PDZD8 Disruption Causes Cognitive Impairment in Humans, Mice, and Fruit Flies. *Biol Psychiatry* **92**, 323-334, doi:10.1016/j.biopsych.2021.12.017 (2022).

26 Kurihara, Y. *et al.* PDZD8-deficient mice manifest behavioral abnormalities related to emotion, cognition, and adaptation due to dyslipidemia in the brain. *Mol Brain* **16**, 11, doi:10.1186/s13041-023-01002-4 (2023).

27 Chan, R. B. *et al.* Comparative lipidomic analysis of mouse and human brain with Alzheimer disease. *J Biol Chem* **287**, 2678-2688, doi:10.1074/jbc.M111.274142 (2012).

28 van der Kant, R. *et al.* Cholesterol Metabolism Is a Druggable Axis that Independently Regulates Tau and Amyloid-beta in iPSC-Derived Alzheimer's Disease Neurons. *Cell Stem Cell* **24**, 363-375 e369, doi:10.1016/j.stem.2018.12.013 (2019).

29 Nugent, A. A. *et al.* TREM2 Regulates Microglial Cholesterol Metabolism upon Chronic Phagocytic Challenge. *Neuron* **105**, 837-854 e839, doi:10.1016/j.neuron.2019.12.007 (2020).

30 Blanchard, J. W. *et al.* APOE4 impairs myelination via cholesterol dysregulation in oligodendrocytes. *Nature* **611**, 769-779, doi:10.1038/s41586-022-05439-w (2022).

31 Guo, J. L. *et al.* Decreased lipidated ApoE-receptor interactions confer protection against pathogenicity of ApoE and its lipid cargoes in lysosomes. *Cell* **188**, 187-206 e126, doi:10.1016/j.cell.2024.10.027 (2025).

32 Mayran, N., Parton, R. G. & Gruenberg, J. Annexin II regulates multivesicular endosome biogenesis in the degradation pathway of animal cells. *EMBO J* **22**, 3242-3253, doi:10.1093/emboj/cdg321 (2003).

33 Lloyd-Evans, E. *et al.* Niemann-Pick disease type C1 is a sphingosine storage disease that causes deregulation of lysosomal calcium. *Nat Med* **14**, 1247-1255, doi:10.1038/nm.1876 (2008).

34 Bissig, C. *et al.* Viral infection controlled by a calcium-dependent lipid-binding module in ALIX. *Dev Cell* **25**, 364-373, doi:10.1016/j.devcel.2013.04.003 (2013).

35 Bretou, M. *et al.* Accumulation of APP C-terminal fragments causes endolysosomal dysfunction through the dysregulation of late endosome to lysosome-ER contact sites. *Dev Cell* **59**, 1571-1592 e1579, doi:10.1016/j.devcel.2024.03.030 (2024).

36 Churchill, G. C. *et al.* NAADP mobilizes Ca(2+) from reserve granules, lysosome-related organelles, in sea urchin eggs. *Cell* **111**, 703-708, doi:10.1016/s0092-8674(02)01082-6 (2002).

37 Calcraft, P. J. *et al.* NAADP mobilizes calcium from acidic organelles through two-pore channels. *Nature* **459**, 596-600, doi:10.1038/nature08030 (2009).

38 Galione, A. A primer of NAADP-mediated Ca(2+) signalling: From sea urchin eggs to mammalian cells. *Cell Calcium* **58**, 27-47, doi:10.1016/j.ceca.2014.09.010 (2015).

39 Kilpatrick, B. S. *et al.* An Endosomal NAADP-Sensitive Two-Pore Ca(2+) Channel Regulates ER-Endosome Membrane Contact Sites to Control Growth Factor Signaling. *Cell Rep* **18**, 1636-1645, doi:10.1016/j.celrep.2017.01.052 (2017).

40 Yuan, Y. *et al.* Two-pore channel-2 and inositol trisphosphate receptors coordinate Ca(2+) signals between lysosomes and the endoplasmic reticulum. *Cell Rep* **43**, 113628, doi:10.1016/j.celrep.2023.113628 (2024).

41 Zheng, Q. *et al.* Calcium transients on the ER surface trigger liquid-liquid phase separation of FIP200 to specify autophagosome initiation sites. *Cell* **185**, 4082-4098 e4022, doi:10.1016/j.cell.2022.09.001 (2022).

42 Ungewickell, A. *et al.* The identification and characterization of two phosphatidylinositol-4,5-bisphosphate 4-phosphatases. *Proc Natl Acad Sci U S A* **102**, 18854-18859, doi:10.1073/pnas.0509740102 (2005).

43 Zou, J., Marjanovic, J., Kisseleva, M. V., Wilson, M. & Majerus, P. W. Type I phosphatidylinositol-4,5-bisphosphate 4-phosphatase regulates stress-induced apoptosis. *Proc Natl Acad Sci U S A* **104**, 16834-16839, doi:10.1073/pnas.0708189104 (2007).

44 Hashimoto, Y., Shirane, M. & Nakayama, K. I. TMEM55B contributes to lysosomal homeostasis and amino acid-induced mTORC1 activation. *Genes Cells* **23**, 418-434, doi:10.1111/gtc.12583 (2018).

45 Xu, H. & Ren, D. Lysosomal physiology. *Annu Rev Physiol* **77**, 57-80, doi:10.1146/annurev-physiol-021014-071649 (2015).

46 Banerjee, S. & Kane, P. M. Regulation of V-ATPase Activity and Organelle pH by Phosphatidylinositol Phosphate Lipids. *Front Cell Dev Biol* **8**, 510, doi:10.3389/fcell.2020.00510 (2020).

47 Ballabio, A. & Bonifacino, J. S. Lysosomes as dynamic regulators of cell and organismal homeostasis. *Nat Rev Mol Cell Biol* **21**, 101-118, doi:10.1038/s41580-019-0185-4 (2020).

515 48 Willett, R. *et al.* TFEB regulates lysosomal positioning by modulating
516 TMEM55B expression and JIP4 recruitment to lysosomes. *Nat Commun* **8**,
517 1580, doi:10.1038/s41467-017-01871-z (2017).
518 49 Jeong, E., Willett, R., Rissone, A., La Spina, M. & Puertollano, R. TMEM55B
519 links autophagy flux, lysosomal repair, and TFE3 activation in response to
520 oxidative stress. *Nat Commun* **15**, 93, doi:10.1038/s41467-023-44316-6 (2024).
521 50 Medina, M. W. *et al.* Transmembrane protein 55B is a novel regulator of cellular
522 cholesterol metabolism. *Arterioscler Thromb Vasc Biol* **34**, 1917-1923,
523 doi:10.1161/ATVBAHA.113.302806 (2014).
524 51 Qin, Y. *et al.* Phosphatidylinositol-(4,5)-Bisphosphate Regulates Plasma
525 Cholesterol Through LDL (Low-Density Lipoprotein) Receptor Lysosomal
526 Degradation. *Arterioscler Thromb Vasc Biol* **40**, 1311-1324,
527 doi:10.1161/ATVBAHA.120.314033 (2020).
528 52 Matsumoto, M. *et al.* Large-scale proteomic analysis of tyrosine-
529 phosphorylation induced by T-cell receptor or B-cell receptor activation reveals
530 new signaling pathways. *Proteomics* **9**, 3549-3563,
531 doi:10.1002/pmic.200900011 (2009).
532 53 Kakimoto, Y. *et al.* Visualizing multiple inter-organelle contact sites using the
533 organelle-targeted split-GFP system. *Sci Rep* **8**, 6175, doi:10.1038/s41598-018-
534 24466-0 (2018).
535 54 Suzuki, J. *et al.* Imaging intraorganellar Ca2+ at subcellular resolution using
536 CEPIA. *Nat Commun* **5**, 4153, doi:10.1038/ncomms5153 (2014).
537 55 Atakpa, P., Thillaiappan, N. B., Mataragka, S., Prole, D. L. & Taylor, C. W.
538 IP(3) Receptors Preferentially Associate with ER-Lysosome Contact Sites and
539 Selectively Deliver Ca(2+) to Lysosomes. *Cell Rep* **25**, 3180-3193 e3187,
540 doi:10.1016/j.celrep.2018.11.064 (2018).
541 56 Otera, H. *et al.* A novel insertion pathway of mitochondrial outer membrane
542 proteins with multiple transmembrane segments. *J Cell Biol* **179**, 1355-1363,
543 doi:10.1083/jcb.200702143 (2007).
544

545 **Acknowledgements and Funding Information**

546 We thank Y. Tamura for split-GFP cDNAs; E. Taylor for Ly-GG cDNA; K. Mihara for
547 Su9 cDNA; K. I. Nakayama and T. Ohnishi for proteome analysis; K. Sato and K. Kato
548 for Ca^{2+} imaging analysis; and the Research Equipment Sharing Center at Nagoya City
549 University for assistance. This work was supported in part by KAKENHI grants from
550 Japan Society for the Promotion of Science (JSPS) to M.S. (24K02122).

Author contributions statement

M.S. designed experiments, supervised the study, analyzed the data, and wrote the manuscript. N.M. and H.M. performed experiments.

Additional information

Data availability

The MS data have been deposited in the JPOST Repository Database as follows:
URL: https://repository.jpostdb.org
JPID and PXID are as follows;
Mock-FLAG complex in Neuro2A; (1) JPST004039, PXD067776; (2) JPST004040, PXD067777; (3) JPST004041, PXD067779.
PDZD8-FLAG complex in Neuro2A; (1) JPST004042, PXD067780; (2) JPST004043, PXD067782; (3) JPST004044, PXD067783.

Supplementary datasets

Raw data are provided within the supplementary information file.

Competing interests

The authors declare no competing interests.

Correspondence

Correspondence and requests for materials should be addressed to M.S. (shiram@phar.nagoya-cu.ac.jp)

577 **Figure Legends**

578 **Fig. 1.** Identification of PDZD8-associated proteins by proteomic analysis. (**A**)
579 Endosome-related proteins identified as PDZD8-associated proteins. Protein abundance
580 was estimated semiquantitatively by identification frequency (IF). Asterisks indicate
581 proteins previously reported as TMEM55B-associated. Lysosome (Ly)-localized and
582 cholesterol (Chol)-related proteins are also indicated. Proteins were categorized based on
583 Gene Ontology (GO) terms and UniProtKB annotations. (**B, C**) HeLa cells were
584 transfected with siControl, siTMEM55B#1, or siTMEM55B#2. Total RNA was analyzed
585 by RT-qPCR for TMEM55B mRNA (B), and protein levels were examined by
586 immunoblotting with anti-TMEM55B and anti-HSP90 antibodies (C). Data are shown as
587 mean ± SE (n = 9 for RNA analysis). ***$p < 0.001$ (one-way ANOVA with Dunnett's
588 multiple comparisons). (**D**) HeLa cells were transfected with siControl, siTMEM55B#1,
589 or siTMEM55B#2 together with split-GFP vectors ERj1–GFP(1–10) and LAMP1–
590 GFP(11), along with mCherry as a transfection control. Scale bar, 10 µm. (**E**)
591 Quantification of split-GFP fluorescence normalized to mCherry intensity as in (D). n =
592 38, 36, and 37 cells for siControl, siTMEM55B#1, and siTMEM55B#2, respectively. n.s.,
593 not significant (Kruskal–Wallis test with Steel's multiple comparisons).
594

595 **Fig. 2.** TMEM55B depletion impairs lysosomal acidification and lipolysis. (**A, C**) HeLa
596 cells transfected with siControl, siTMEM55B#1, or siTMEM55B#2 were stained with
597 LysoTracker Red (A) or LysoSensor Green (C) and analyzed by confocal microscopy.
598 Boxed areas (top panels) are shown at higher magnification (bottom panels). Scale bars,
599 10 µm (top and middle) and 5 µm (bottom). (**B, D**) Quantification of LysoTracker Red
600 (B) or LysoSensor Green (D) mean fluorescence intensity per lysosome in (A) (n = 746,
601 497, and 452 lysosomes for siControl, siTMEM55B#1, and siTMEM55B#2,
602 respectively) or (C) (n = 703, 847, and 794 lysosomes, respectively). (**E**) RT-qPCR
603 analysis of TMEM55B mRNA in PC12 cells transfected with siControl, siTMEM55B#1,
604 or siTMEM55B#2 (mean ± SE, n = 6). (**F**) PC12 cells were transfected with siControl,
605 siTMEM55B#1, or siTMEM55B#2 together with EGFP-PLIN2, and stained with
606 LysoTracker Red. (**G**) Quantification of lipid droplet (LD) size (µm²) of EGFP-PLIN2
607 puncta in (F) (n = 627, 450, and 317 LDs for siControl, siTMEM55B#1, and
608 siTMEM55B#2, respectively). (**H**) Quantification of mean EGFP-PLIN2 fluorescence
609 intensity per cell in (F) (n = 52, 41, and 35 cells for siControl, siTMEM55B#1, and
610 siTMEM55B#2, respectively). (**I**) Quantification of mean LysoTracker Red fluorescence
611 intensity per cell in (F) (n = 52, 41, and 35 cells, respectively). (**J**) Pearson's correlation
612 coefficient between EGFP-PLIN2 and LysoTracker Red per cell in (F) (n = 52, 41, and

613 35 cells, respectively). ***p < 0.001, **p < 0.01 (Kruskal–Wallis test with Steel's
614 multiple comparisons test in B, D, and G–I); **p < 0.01, *p < 0.05 (one-way ANOVA
615 with Dunnett's multiple comparisons in E and J).
616
617 **Fig. 3.** Depletion of TMEM55B impairs Ca^{2+} release from the ER. (**A**) Schematic
618 representation of G-CEPIA1er, a Ca^{2+} indicator with the G-GECO1 domain facing the
619 ER lumen. (**B**) Confocal images of HeLa cells co-expressing G-CEPIA1er (green) and
620 the ER marker mCherry-KDEL (red). Scale bar, 10 μm. (**C**) Time lapse analysis of G-
621 CEPIA1er fluorescence ($\Delta F/F_0$) in cells transfected with siControl (gray, n = 30 fields),
622 siTMEM55B#1 (red, n = 30), or siTMEM55B#2 (pink, n = 30). ATP (200 μM) was added
623 at t = 0 s; Data are mean ± SE. (**D**) Quantification of peak $\Delta F/F_0$ values in (C).
624 (**E**) Quantification of the slope of G-CEPIA1er $\Delta F/F_0$ during 0–120 s after ATP addition
625 ($\Delta F/F_0 \cdot s^{-1}$). (**F**) Quantification of time (s) to peak after ATP addition for G-CEPIA1er
626 $\Delta F/F_0$. (**G**) Quantification of the slope of G-CEPIA1er $\Delta F/F_0$ during 900 s after the peak
627 ($\Delta F/F_0 \cdot s^{-1}$). Data are mean ± SE; ***p < 0.001, *p < 0.05 (Kruskal–Wallis test with
628 Steel's multiple comparisons in D, F, and G); ***p < 0.001 (one-way ANOVA with
629 Dunnett's multiple comparisons in E).
630
631 **Fig. 4.** Depletion of TMEM55B impairs lysosomal Ca^{2+} dynamics. (**A**) Schematic
632 representation of Ly-GG, a Ca^{2+} indicator with the G-GECO1 domain facing the cytosolic
633 side of the lysosomal membrane. (**B**) Confocal images of HeLa cells co-expressing Ly-
634 GG (green) and the lysosomal marker mCherry–LAMP1 (red). Scale bar, 10 μm. (**C**)
635 Time lapse analysis of Ly-GG fluorescence ($\Delta F/F_0$) in cells transfected with siControl
636 (gray, n = 29 fields), siTMEM55B#1 (red, n = 29), or siTMEM55B#2 (pink, n = 26). ATP
637 (200 μM) was added at t = 0 s; Data are mean ± SE and normalized by subtracting values
638 from ATP-free cells, in which fluorescence declined due to photobleaching. (**D, E**)
639 Quantification of Ly-GG slopes during 0–60 s (D) and 60–160 s (E) ($\Delta F/F_0 \cdot s^{-1}$). (**F**)
640 Schematic representation of CEPIA3mt, a Ca^{2+} indicator with the GCaMP2 domain
641 facing the mitochondrial matrix. (**G**) Confocal images of HeLa cells co-expressing
642 CEPIA3mt (green) and the mitochondrial marker Su9–RFP (red). Scale bar, 10 μm. (**H**)
643 Time lapse analysis of CEPIA3mt fluorescence ($\Delta F/F_0$) in cells transfected with control
644 siRNA (gray, n = 25 fields), siTMEM55B#1 (red, n = 26), or siTMEM55B#2 (pink, n =
645 24). ATP (200 μM) was added at t = 0 s; Data are mean ± SE. (**I, J**) Quantification of
646 CEPIA3mt slopes during 0–60 s (I) and 60–160 s (J) ($\Delta F/F_0 \cdot s^{-1}$). Data are mean ± SE;
647 ***p < 0.001; (Kruskal–Wallis test with Steel's multiple comparisons in D and E); n.s.,
648 not significant (one-way ANOVA with Dunnett's multiple comparisons in I and J).

649

650 **Fig. 5.** Model of the mechanism where TMEM55B promotes lipolysis via lysosomal
651 acidification and calcium regulation at ER-Ly MCSs. ER protein PDZD8 is associated
652 with lysosome protein TMEM55B that promotes lysosomal acidification through
653 regulation of v-ATPase. Lysosomal acidification then promotes activity of lysosomal
654 acidic lipases that promote lipolysis and subsequently degradation of CEs to cholesterol,
655 as well as calcium channels that promote CICR. CICR at ER-Ly MCSs may also
656 contribute to lipolysis by fusion of LDs or LPs with lysosomes. ER, endoplasmic
657 reticulum; MCS, membrane contact site; v-ATPase, vacuolar-ATPase; TPC2, two-pore
658 channel 2; TRPML1, transient receptor potential mucolipin 1; RyR, ryanodine receptor;
659 IP_3R, inositol 1,4,5-trisphosphate receptor; CICR, Ca^{2+}-induced Ca^{2+} release; LD, lipid
660 droplet; LP, lipoprotein; CE, cholesteryl ester; Chol, cholesterol.
661

A

Gene symbol	Protein name	IF	Ly	Chol
Zfyve27	ISOFORM 1 OF ZINC FINGER FYVE DOMAIN-CONTAINING PROTEIN 27.	1.095		
Stmn2	STATHMIN-2.	0.500		
Vac14	PROTEIN VAC14 HOMOLOG.	0.324		
**Atp6v0d1*	VACUOLAR PROTON PUMP SUBUNIT D 1.	0.200	✓	
Sh3gl1	ENDOPHILIN-A2.	0.125		
Gm364	SIMILAR TO TRANSMEMBRANE 9 SUPERFAMILY MEMBER 2.	0.111		
**Lamtor1*	UPF0404 PROTEIN C11ORF59 HOMOLOG.	0.111	✓	✓
Tfrc	TRANSFERRIN RECEPTOR PROTEIN 1.	0.100		
**Tmem55b*	TRANSMEMBRANE PROTEIN 55B.	0.083	✓	✓
Fig4	SAC DOMAIN-CONTAINING PROTEIN 3.	0.048		
Sun2	PROEIN UNC-84 HOMOLOG B.	0.032		
Vps35	VACUOLAR PROTEIN SORTING-ASSOCIATED PROTEIN 35.	0.026	✓	
Kif13a	KINESIN-LIKE PROTEIN KIF13A.	0.014		

B

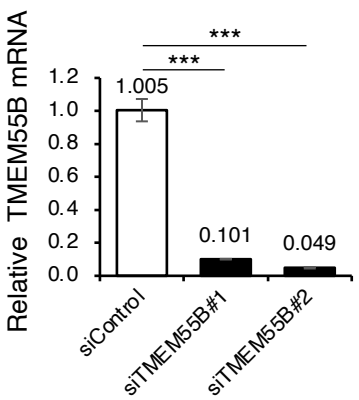

C

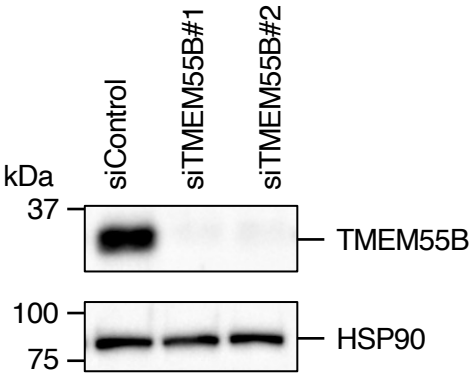

D

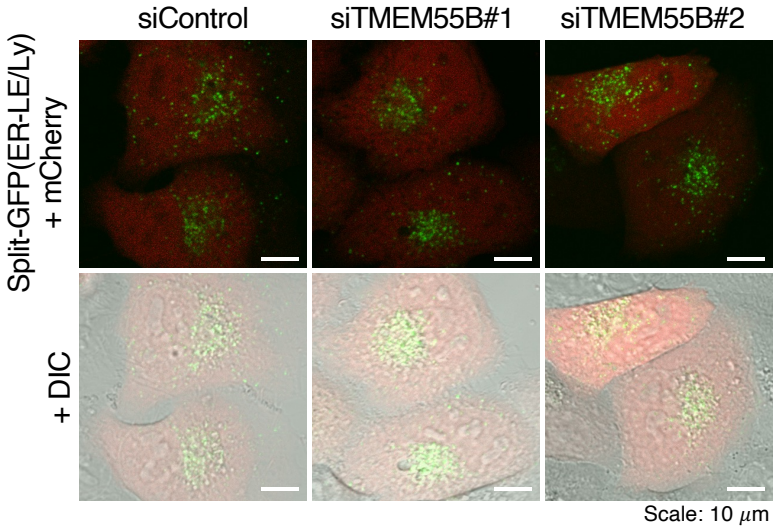

E

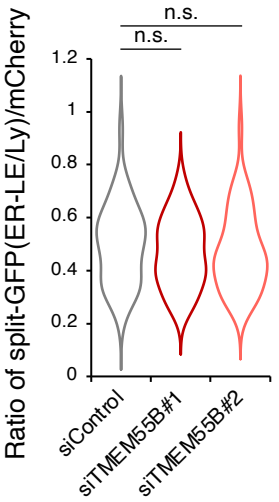

Figure 1

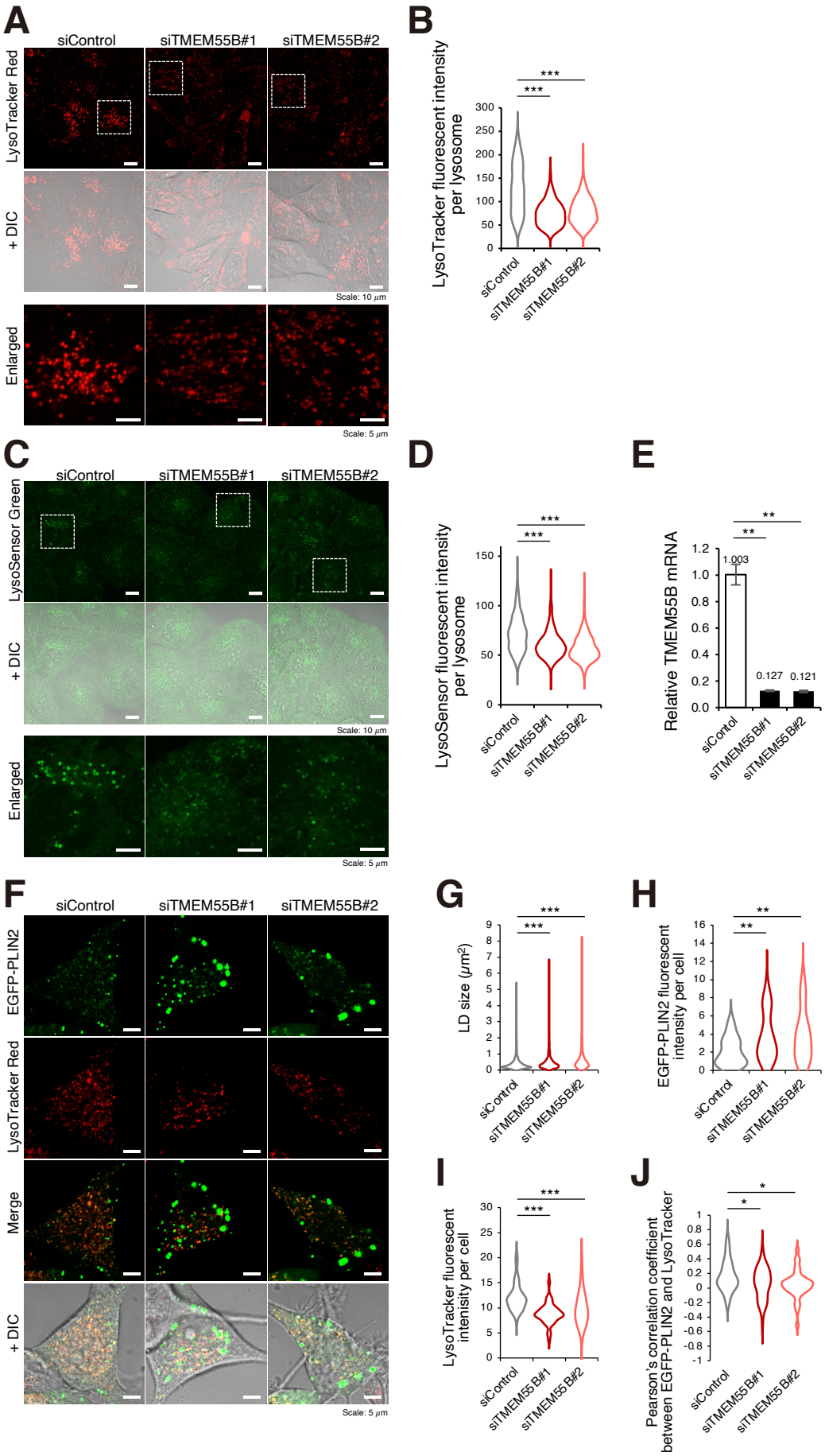
A
siControl
siTMEM55B#1
siTMEM55B#2
LysoTracker Red
+ DIC
Enlarged
Scale: 10 μm
Scale: 5 μm
B
LysoTracker fluorescent intensity per lysosome
***
***
siControl
siTMEM55B#1
siTMEM55B#2
C
LysoSensor Green
D
LysoSensor fluorescent intensity per lysosome
E
Relative TMEM55B mRNA
1.003
0.127
0.121
**
F
EGFP-PLIN2
Merge
G
LD size (μm²)
H
EGFP-PLIN2 fluorescent intensity per cell
I
LysoTracker fluorescent intensity per cell
J
Pearson's correlation coefficient between EGFP-PLIN2 and LysoTracker
*

Figure 2

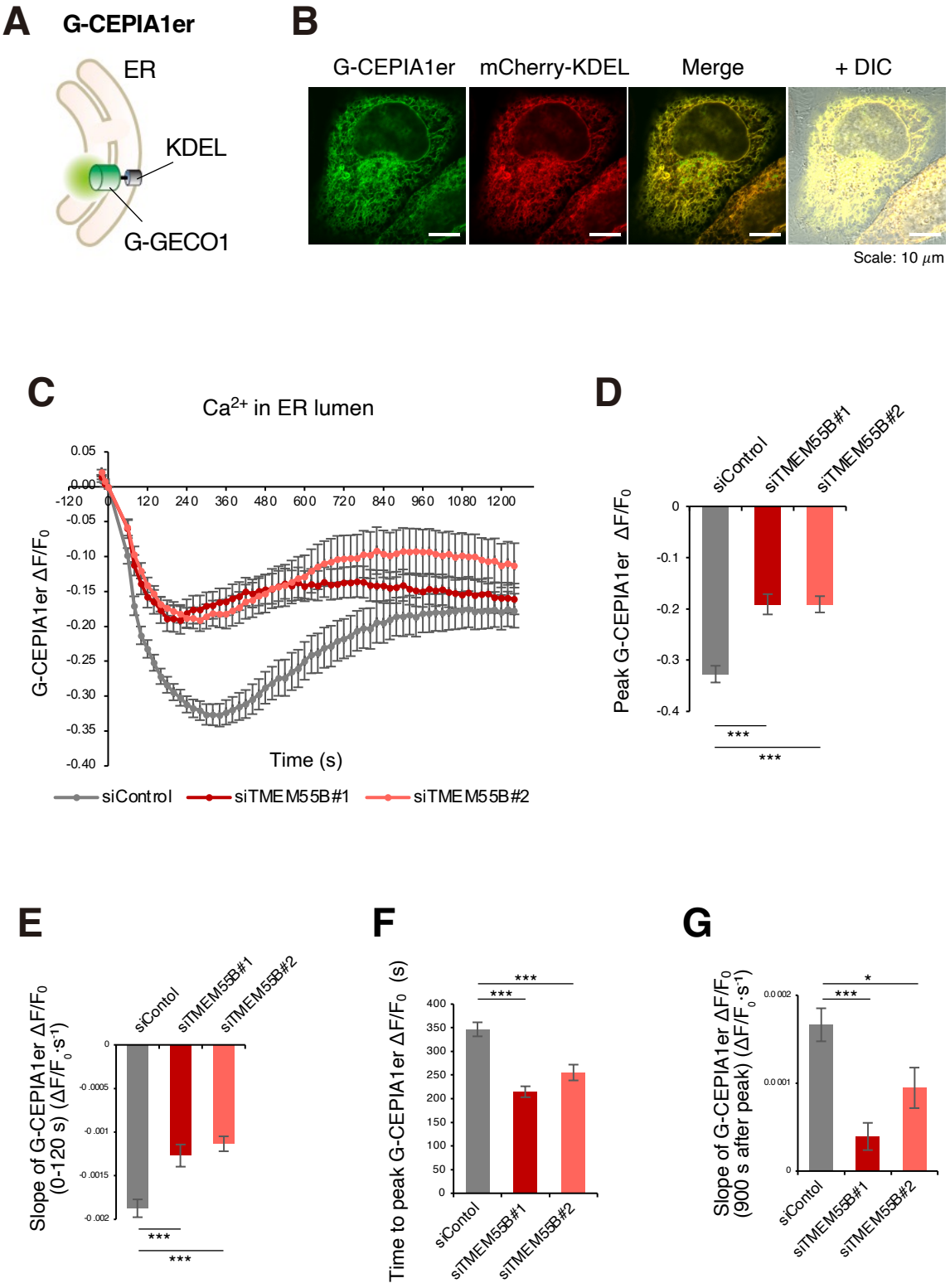
A
G-CEPIA1er
ER
KDEL
G-GECO1
B
G-CEPIA1er
mCherry-KDEL
Merge
+ DIC
Scale: 10 μm
C
Ca2+ in ER lumen
G-CEPIA1er ΔF/F0
Time (s)
siControl
siTMEM55B#1
siTMEM55B#2
D
Peak G-CEPIA1er ΔF/F0
siControl
siTMEM55B#1
siTMEM55B#2
***
***
E
Slope of G-CEPIA1er ΔF/F0 (0-120 s) (ΔF/F0·s-1)
siContol
siTMEM55B#1
siTMEM55B#2
***
***
F
Time to peak G-CEPIA1er ΔF/F0 (s)
siContol
siTMEM55B#1
siTMEM55B#2
***
***
G
Slope of G-CEPIA1er ΔF/F0 (900 s after peak) (ΔF/F0·s-1)
siContol
siTMEM55B#1
siTMEM55B#2
*
***

Figure 3

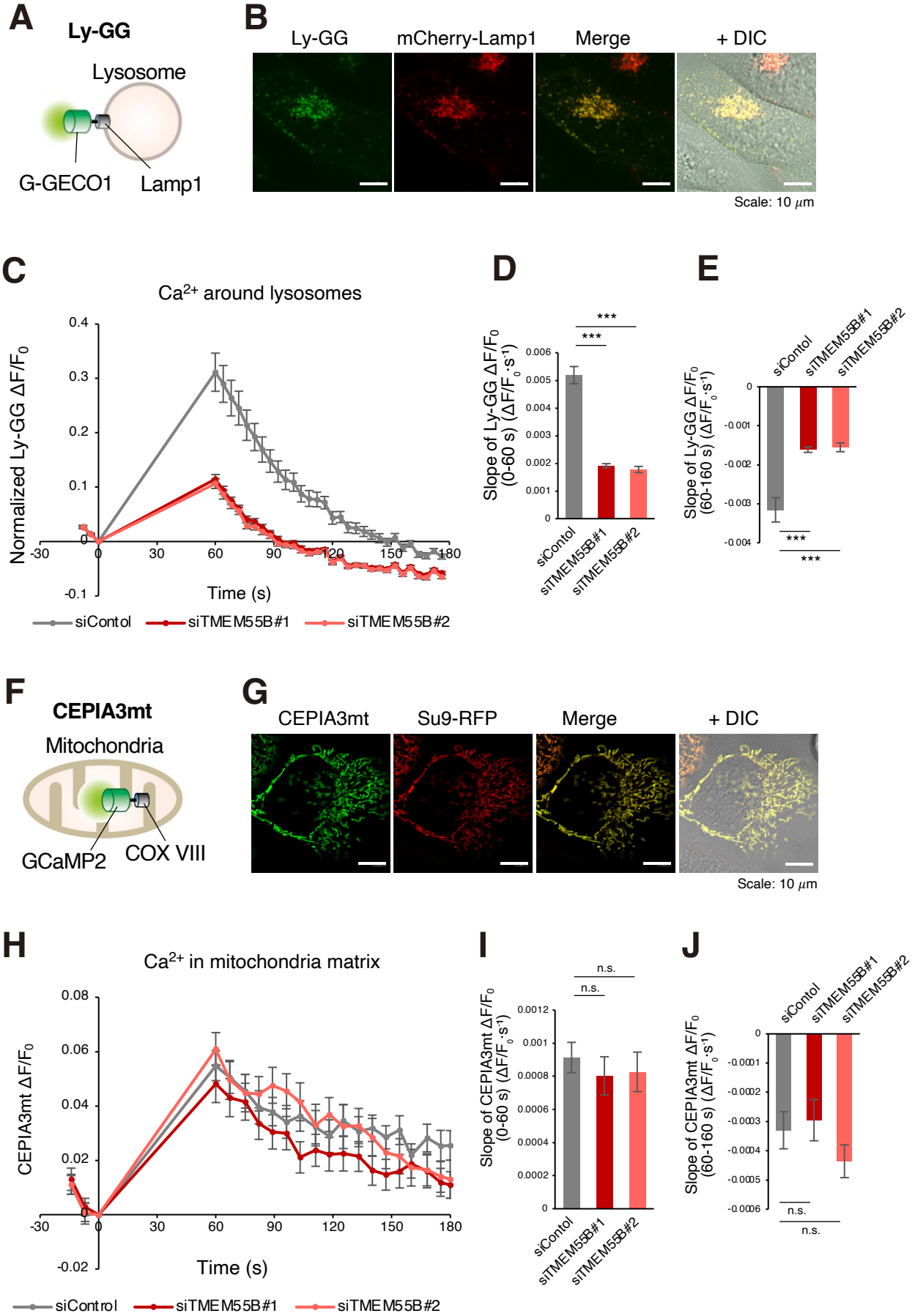
A
Ly-GG
Lysosome
G-GECO1
Lamp1
B
Ly-GG
mCherry-Lamp1
Merge
+ DIC
Scale: 10 μm
C
Ca2+ around lysosomes
Normalized Ly-GG ΔF/F0
Time (s)
siContol
siTMEM55B#1
siTMEM55B#2
D
Slope of Ly-GG ΔF/F0 (0-60 s) (ΔF/F0·s-1)
***
***
siContol
siTMEM55B#1
siTMEM55B#2
E
Slope of Ly-GG ΔF/F0 (60-160 s) (ΔF/F0·s-1)
siContol
siTMEM55B#1
siTMEM55B#2
***
***
F
CEPIA3mt
Mitochondria
GCaMP2
COX VIII
G
CEPIA3mt
Su9-RFP
Merge
+ DIC
Scale: 10 μm
H
Ca2+ in mitochondria matrix
CEPIA3mt ΔF/F0
Time (s)
siControl
siTMEM55B#1
siTMEM55B#2
I
Slope of CEPIA3mt ΔF/F0 (0-60 s) (ΔF/F0·s-1)
n.s.
n.s.
siContol
siTMEM55B#1
siTMEM55B#2
J
Slope of CEPIA3mt ΔF/F0 (60-160 s) (ΔF/F0·s-1)
siContol
siTMEM55B#1
siTMEM55B#2
n.s.
n.s.

Figure 4

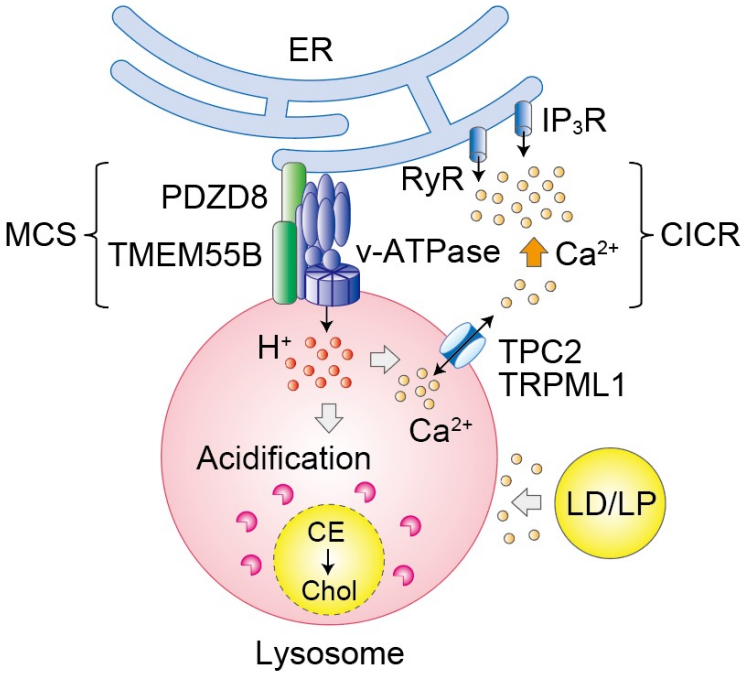
ER
IP3R
RyR
PDZD8
MCS
TMEM55B
v-ATPase
Ca2+
CICR
H+
TPC2
TRPML1
Ca2+
Acidification
LD/LP
CE
Chol
Lysosome

Figure 5